




ER-anchored CRTH2 antagonizes collagen biosynthesis and organ fibrosis via binding LARP6

Shengkai Zuo¹, Bei Wang¹, Jiao Liu¹, Deping Kong¹, Hui Cui², Yaonan Jia³, Chenyao Wang⁴, Xin Xu¹ , Guilin Chen¹, Yuanyang Wang¹, Linlin Yang⁵, Kai Zhang⁶, Ding Ai⁷, Jie Du⁸, Yujun Shen^{1,*}  & Ying Yu^{1,**} 

Abstract

Excessive deposition of extracellular matrix, mainly collagen protein, is the hallmark of organ fibrosis. The molecular mechanisms regulating fibrotic protein biosynthesis are unclear. Here, we find that chemoattractant receptor homologous molecule expressed on TH2 cells (CRTH2), a plasma membrane receptor for prostaglandin D₂, is trafficked to the endoplasmic reticulum (ER) membrane in fibroblasts in a caveolin-1-dependent manner. ER-anchored CRTH2 binds the collagen mRNA recognition motif of La ribonucleoprotein domain family member 6 (LARP6) and promotes the degradation of collagen mRNA in these cells. In line, CRTH2 deficiency increases collagen biosynthesis in fibroblasts and exacerbates injury-induced organ fibrosis in mice, which can be rescued by LARP6 depletion. Administration of CRTH2 N-terminal peptide reduces collagen production by binding to LARP6. Similar to CRTH2, bumetanide binds the LARP6 mRNA recognition motif, suppresses collagen biosynthesis, and alleviates bleomycin-triggered pulmonary fibrosis *in vivo*. These findings reveal a novel anti-fibrotic function of CRTH2 in the ER membrane via the interaction with LARP6, which may represent a therapeutic target for fibrotic diseases.

Keywords collagen synthesis; CRTH2; LARP6; organ fibrosis

Subject Category Membranes & Trafficking

DOI 10.15252/emboj.2020107403 | Received 27 November 2020 | Revised 11 May 2021 | Accepted 20 May 2021 | Published online 5 July 2021

The EMBO Journal (2021) 40: e107403

Introduction

Fibrosis is the common pathological feature of many chronic inflammatory diseases. It affects virtually all tissues and organs in the body. Histologically, fibrosis is characterized by the accumulation of excess extracellular matrix (ECM) materials, such as collagen and fibronectin, in the inflamed or damaged tissues. Although this fibrotic response is an indispensable and reversible process for wound healing, if it persists as chronic inflammation or if tissue is severely injured, fibrosis can progressively become irreversible and ultimately lead to organ malfunction and death. Despite considerable progress in the understanding of the molecular signals and cellular mechanisms underlying fibrosis, there are still few effective clinical therapies targeting fibrogenesis (Weiskirchen *et al*, 2019).

In parenchymal organs, tissue damage that includes toxicity or infection leads to an inflammatory reaction by recruiting a variety of immune cells and releasing different biologically active mediators (cytokines and chemokines). The infiltrated immune cells elicit the activation of effector cells, which prime the fibrogenic process. Fibroblasts and differentiated myofibroblasts are the main fibrotic effector cell response for ECM synthesis in many organs (Wynn & Ramalingam, 2012; Rockey *et al*, 2015). Various precursor cell populations can transit into myofibroblasts or matrix-producing cells. However, resident fibroblasts appear to be the predominant contributing source of myofibroblasts and the resulting tissue fibrosis in diseases, such as systemic sclerosis and idiopathic pulmonary fibrosis (Kendall & Feghali-Bostwick, 2014). Thus, targeting fibroblasts may be a promising option for the treatment of organ fibrosis. Chemoattractant receptor homologous molecule expressed on TH2 cells (CRTH2) is the cell membrane receptor for prostaglandin D₂ (PGD₂). CRTH2 is highly expressed in type 2 helper T cells (Th₂), innate lymphoid cells, eosinophils, and

1 Tianjin Key Laboratory of Inflammatory Biology, Center for Cardiovascular Diseases, Key Laboratory of Immune Microenvironment and Disease (Ministry of Education), Department of Pharmacology, The Province and Ministry Co-sponsored Collaborative Innovation Center for Medical Epigenetics, School of Basic Medical Sciences, Tianjin Medical University, Tianjin, China

2 School of Life Science and Technology, Shanghai Tech University, Shanghai, China

3 School of Pharmaceutical Sciences, Zhengzhou University, Zhengzhou, China

4 Department of Inflammation and Immunity, Lerner Research Institute, Cleveland Clinic, Cleveland, OH, USA

5 Department of Pharmacology, School of Basic Medical Sciences, Zhengzhou University, Zhengzhou, China

6 Department of Biochemistry and Molecular Biology, School of Basic Medical Sciences, Tianjin Medical University, Tianjin, China

7 Department of Physiology and Pathophysiology, School of Basic Medical Sciences, Tianjin Medical University, Tianjin, China

8 Beijing Anzhen Hospital of Capital Medical University and Beijing Institute of Heart Lung and Blood Vessel Diseases, Beijing, China

*Corresponding author. Tel: +86 22 83336642; E-mail: yujun_shen@tmu.edu.cn

**Corresponding author. Tel: +86 22 83336627; E-mail: yuying@tmu.edu.cn

basophils (Hirai *et al*, 2001). The PGD₂/CRTH2 axis is involved in type 2 inflammation reactions that occur in asthma and allergic rhinitis (Kupczyk & Kuna, 2017; Marone *et al*, 2019). Inhibition of CRTH2-mediated Th2 activation ameliorates unilateral ureteral obstruction (UUO)-induced renal fibrosis (Ito *et al*, 2012). In contrast, genetic deficiency of CRTH2 aggravates bleomycin-induced pulmonary fibrosis in mice, accompanied by reduced infiltration of $\gamma\delta$ T cells in the lungs (Ito *et al*, 2012; Ueda *et al*, 2019). These observations indicate that CRTH2 in different inflammatory cells may function differently in organ fibrogenesis. We and others have found that CRTH2 is also highly expressed in fibroblasts (Maruyama *et al*, 2008; Zuo *et al*, 2018a). However, the exact role of CRTH2 in fibroblasts remains unknown in organ fibrosis.

In this study, we observed CRTH2 located unexpectedly in endoplasmic reticulum (ER) membrane in fibroblasts, and the ER-anchored CRTH2 suppressed collagen biosynthesis in fibroblasts through binding La ribonucleoprotein domain family member 6 (LARP6) at the RNA recognition motif (RRM). Bumetanide inhibited TGF- β 1-induced collagen expression in fibroblasts and reduced bleomycin-induced pulmonary fibrosis in mice by mimicking the structurally binding of CRTH2 with LARP6. These observations indicate that CRTH2 regulates collagen biogenesis in fibroblasts by targeting LARP6 in the ER.

Results

CRTH2 is sustained on the ER membrane in fibroblasts by caveolin-1

As a G protein-coupled receptor (GPCR), CRTH2 was located in the cell membrane in all cell lines tested (Fig 1A). Interestingly, CRTH2 colocalized with calnexin in the ER membrane in HEK293T, human fibroblasts MRC-5, NIH 3T3, and primary mouse organ fibroblasts (Fig 1A). Western blot analysis verified CRTH2 protein expression in both cytoplasmic and ER membranes in HEK293T and NIH3T3 cells (Fig 1B). We envision ER CRTH2 may be trafficked originally from cell membrane in fibroblasts.

Scaffold proteins, such as β -arrestins (β -arrestin-1 and β -arrestin-2) and caveolins (caveolin-1 and caveolin-2), are involved in the mediation of the trafficking of GPCRs (Shenoy & Lefkowitz, 2011; Busija *et al*, 2017). We observed that caveolin-1 and caveolin-2 were highly expressed, while expressions of β -arrestin-1 and β -arrestin-2 were relatively low in NIH 3T3 fibroblasts (Fig EV1A). Knockdown of β -arrestin-1 or β -arrestin-2 (Fig EV1B and C) did not markedly influence CRTH2 expression on the ER and fibroblast membranes (Fig EV1D and E). However, caveolin-1 knockdown reduced the ER distribution, but increased plasma membrane distribution, of CRTH2 (Fig EV1F–H), while overexpression of caveolin-1 increased CRTH2 accumulation on ER in fibroblasts (Fig EV1I). Density gradient ultracentrifugation further demonstrated colocalization of CRTH2 and caveolin-1 in lipid rafts (Fig EV1J). TGF- β 1 treatment suppressed caveolin-1 protein in fibroblasts (Fig 1C), consistent with a previous report (Wang *et al*, 2006a). TGF- β 1 stimulation reduced ER trafficking of CRTH2 protein from cell membrane in fibroblasts (Fig 1D and E). Using HA-tagged CRTH2 mice (Appendix Fig S1A and B), we found that TGF- β 1 also inhibited the endogenous CRTH2 translocation in fibrocytes (collagen-

1⁺CD45⁺CXCR4⁺) (Appendix Fig S1C and D)–bone marrow-derived fibroblast precursors (Reilkoff *et al*, 2011). Indeed, pro-fibrotic growth factor PDGF-BB (Leask, 2010) reduced, while anti-fibrotic cytokine IL-10 (Nakagome *et al*, 2006) promoted the ER trafficking of CRTH2 in fibroblasts (Appendix Fig S2A and B). The collective results indicate that caveolin-1 mediates CRTH2 trafficking from the cytoplasmic membrane to the ER membrane in fibroblasts.

Activation of CRTH2 on plasma membrane triggers intracellular Ca²⁺ mobilization into the cytosol (Zuo *et al*, 2018b). However, inhibition of caveolin-1 by genistein did not influence CRTH2 agonist DK-PGD₂-boosted cytosolic Ca²⁺ signals in fibroblasts (Appendix Fig S3A), but did reduce the localization of CRTH2 on ER (Appendix Fig S3B). Moreover, CRTH2 receptor antagonist CAY10595 attenuated DK-PGD₂-induced Ca²⁺ flux (Appendix Fig S3A), but had no effect on ER distribution of CRTH2 in fibroblasts (Appendix Fig S3B). Thus, CRTH2 on ER mediates different cellular signaling from that on plasma membrane in fibroblasts.

CRTH2 interacts with LARP6 RRM in the ER membrane

To investigate the physiological role of ER CRTH2 in fibroblasts, we tried to identify CRTH2-associated proteins in the ER membrane using co-immunoprecipitation (co-IP) and mass spectrometry (MS). Co-IP revealed the CRTH2 formed a complex with LARP6 and the 78-kDa glucose-regulated protein (GRP78) (Fig 2A–D). Western blot assay followed by co-IP and immune staining confirmed the interaction of CRTH2 with LARP6 in the ER membrane (Fig 2E–G). GPR78 is a chaperone protein located in the ER organelle (Wang *et al*, 2009). Binding of CRTH2 to GPR78 at the ER was evident (Fig 2H–J). Thus, CRTH2, LARP6, and GRP78 formed a protein complex in the ER organelle. To determine the structural basis for the interaction of the three proteins, we constructed a series of truncated fragments fused with different tags that included glutathione S-transferase (GST), 3 \times Flag-streptavidin-binding peptide (Flag-SBP), and Myc (Fig EV2A). Protein pull-down assays revealed that an N-terminal region of CRTH2 comprising amino acids 1–36 interacted with the LARP6 RNA RRM in 293T cells (Fig EV2B and C). The interaction was verified by an in vitro binding assay with purified recombinant proteins (Fig EV2D and E). Similarly, we observed that the C-terminal region of CRTH2 directly bound to the substrate binding domain (SBD) of GPR78 (Fig EV2F–I). Despite the association of GRP78 and LARP6 that was evident using the pull-down assay (Appendix Fig S4A and B), direct binding of these two proteins was not detected (Appendix Fig S4C and D). These observations suggest CRTH2 is anchored in the ER by GPR78 and interacts with cytoplasmic LARP6 (Fig 2K).

CRTH2 inhibits collagen synthesis in fibroblasts through LARP6

LARP6 regulates the stability of collagen mRNAs through the RRM binding of the 5' untranslated region (UTR) of these mRNAs (Zhang & Stefanovic, 2016a). Presently, CRTH2 bound competitively to the RRM of LARP6 in the ER membrane (Fig 2). CRTH2 deletion promoted LARP6 binding with collagen mRNAs [collagen type 1, α 1 (Col1a1), collagen type 1, α 2 (Col1a2), and collagen type 3, α 1 (Col3a1)] (Fig 3A) and subsequently suppressed cellular decay of collagen mRNAs and prolonged their half-lives in mouse primary lung fibroblasts (Fig 3B). The mRNA and protein expressions of collagen I and III were increased in mouse fibroblasts (Fig 3C and D).

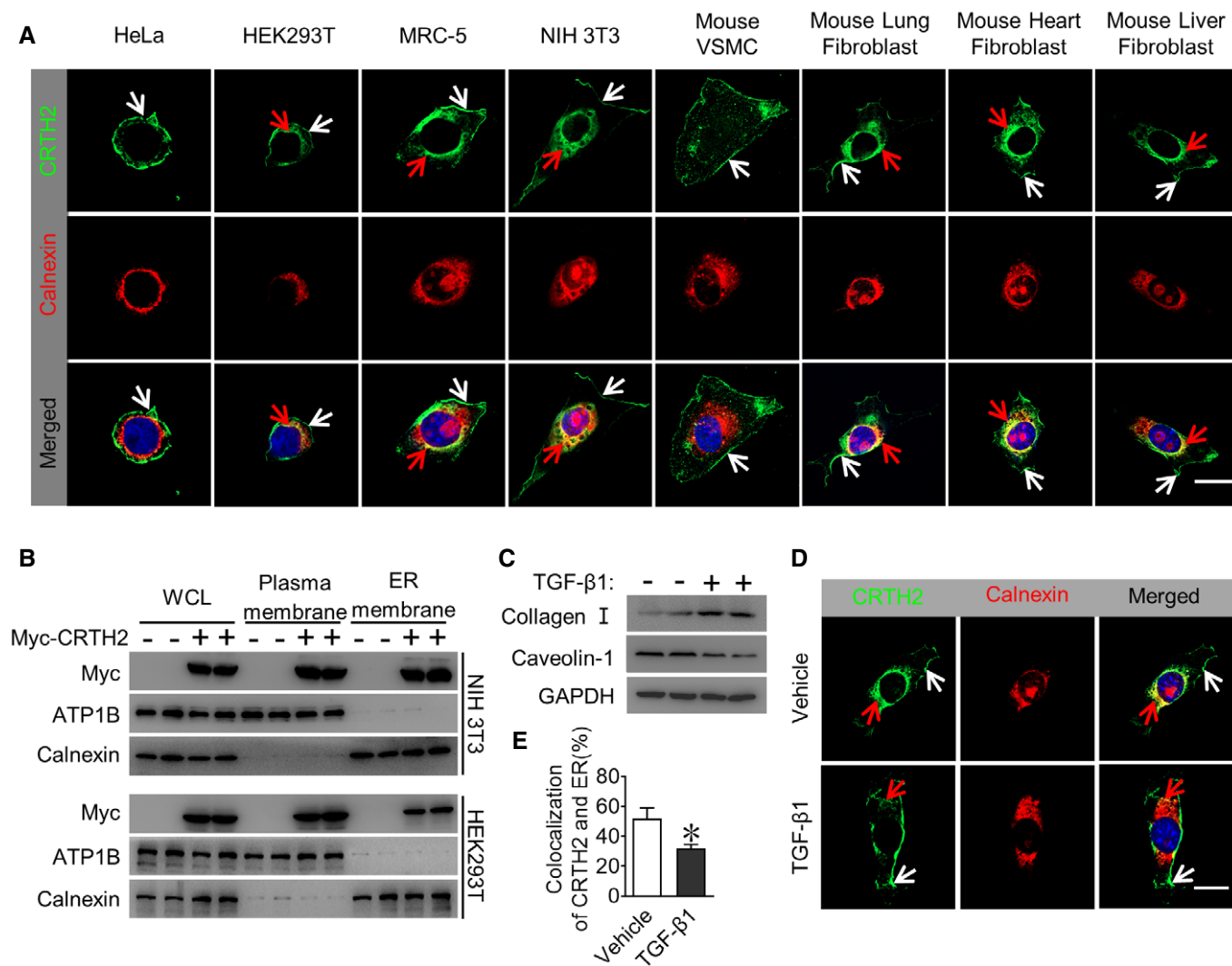


Figure 1. CRTH2 is located in the endoplasmic reticulum (ER) and cell membrane in fibroblasts.

- A CRTH2 subcellular localization in GFP-fused CRTH2-expressing plasmid-transfected cells. Red arrows indicate CRTH2 localized in the ER, and white arrows indicate CRTH2 localized in the plasma membrane. Green, GFP-CRTH2; blue, DAPI; and red, calnexin. Scale bar, 20 μ m.
- B Western blot analysis of CRTH2 expression in cell membrane and ER in NIH 3T3 and HEK293T cells. Myc-tagged CRTH2-expressing plasmid was transfected into NIH 3T3 and HEK293T cells. Whole-cell lysate, plasma, and ER fractions were obtained 48 h after transfection. Calnexin and ATP1B were used as markers for ER and cell membrane, respectively.
- C The effect of TGF- β 1 (10 ng/ml) on the expression of caveolin-1 in NIH 3T3 cells.
- D Representative images of CRTH2 subcellular localization in NIH 3T3 cells in response to TGF- β 1 (10 ng/ml) treatment. Red arrows indicate CRTH2 localized in the ER, and white arrows indicate CRTH2 localized in the plasma membrane. Green, GFP-CRTH2; blue, DAPI; and red, calnexin. Scale bar, 20 μ m.
- E Quantification of CRTH2 colocalization with endoplasmic reticulum after TGF- β 1 or vehicle treatment. * P < 0.05 vs vehicle (Mann-Whitney U-test); n = 4 for all groups. Data are expressed as the mean \pm standard error of the mean.

Source data are available online for this figure.

Knockdown of LARP6 (Fig 3E) markedly diminished the increased stability of collagen mRNAs (Fig 3F) and augmented the expression of collagen I and III in mouse CRTH2^{-/-} fibroblasts (Fig 3G–J). In addition, GRP78 knockdown had no significant influence on the ER distribution of CRTH2 in NIH 3T3 cells and the expressions of collagen I and III in CRTH2^{-/-} fibroblasts (Appendix Fig S5). Interestingly, treatment using the CRTH2 agonist 13, 14-dihydro-15-keto (DK)-PGD₂, a stable metabolite of PGD₂, did not alter the collagen mRNA and protein levels in mouse lung fibroblasts with or without TGF- β 1

stimulation (Fig EV3A–D). In contrast, forced overexpression of CRTH2 reduced collagen I and III expression in fibroblasts (Fig EV3E) and fibrocytes (Fig EV3F). Again, forced expression of caveolin-1 promoted, but caveolin-1 inhibitor genistein diminished, the inhibitory effect of CRTH2 on collagen biosynthesis in fibroblasts (Fig EV3G and H). CRTH2 receptor antagonist CAY10595 had no overt effect on collagen expression (Fig EV3H). Taken together, these results indicated that CRTH2 inhibits LARP6-mediated collagen biosynthesis in fibroblasts in CRTH2 agonist-independent manner.

Fibroblast-specific CRTH2 deficiency exaggerates injury-induced organ fibrosis in mice by increasing LARP6-mediated collagen biosynthesis

To investigate the role of CRTH2 in organ fibrosis, we generated fibroblast-specific CRTH2 deficient mice [F-CRTH2 knockout (KO)] by crossing CRTH2-floxed mice (CRTH2^{lox/flox}) to tamoxifen-

inducible Col1a2 Cre (Col1a2-Cre^{ERT}) transgenic mice (Appendix Fig S6A and B). qRT-PCR demonstrated that the CRTH2 gene was specifically excised in primary fibroblasts in F-CRTH2 KO mice (Appendix Fig S6C). We tested three common experimental mouse models of organ fibrosis: bleomycin-induced pulmonary fibrosis, carbon tetrachloride (CCl₄)-induced liver fibrosis, and isoproterenol-induced cardiac fibrosis. Histological and biochemical analyses

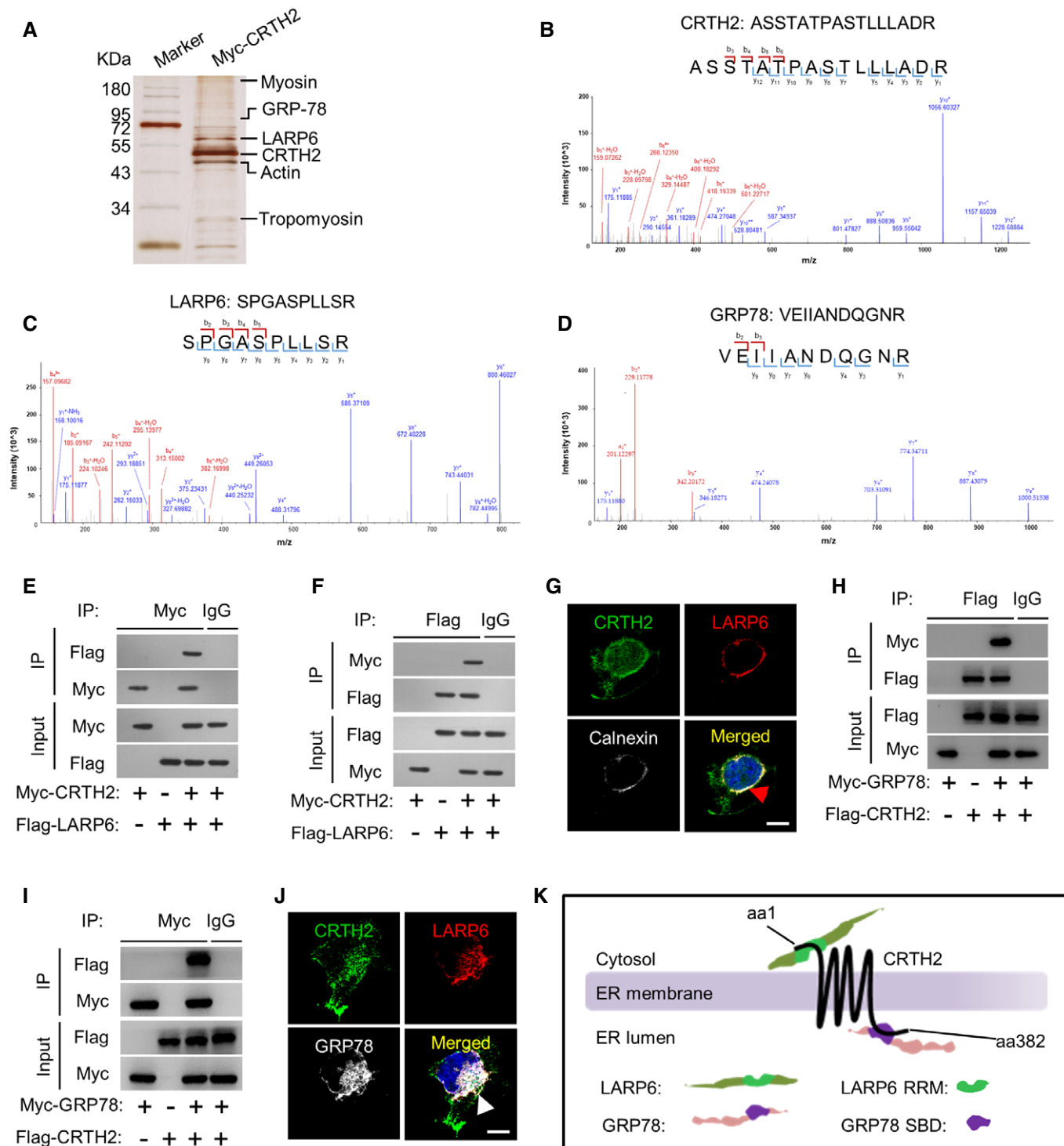


Figure 2. CRTH2 interacts with LARP6 and GRP78 in the ER.

- A Immunopurification and mass spectrometric analysis of CRTH2-containing protein complex in NIH 3T3 cells. Cellular extracts from NIH 3T3 cells stably expressing myc-CRTH2 protein were immunopurified with anti-myc affinity beads and eluted with myc peptide. The eluates were used for SDS-PAGE, and the gels were silver-stained and analyzed using mass spectrometry.
- B–D Representative mass spectrogram of CRTH2 (B), LARP6 (C), and GRP78 (D) from CRTH2-containing protein complex in NIH 3T3 cells.
- E, F Co-immunoprecipitation analysis of association of CRTH2 with LARP6. HEK293T cells were co-transfected with Myc-CRTH2- and Flag-LARP6-expressing plasmids. Whole-cell lysates from HEK293T cells were immunoprecipitated and then immunoblotted with the indicated antibodies.
- G Subcellular localization of CRTH2 and LARP6 in NIH 3T3 cells. NIH 3T3 cells were transfected with GFP-fused CRTH2-expressing plasmid and fixed and immunostained with antibodies against the indicated proteins. Red arrow indicates colocalization of CRTH2 and LARP6 in the ER. Scale bar, 20 μ m.
- H, I Co-IP analysis of association of CRTH2 with GRP78. HEK293T cells were co-transfected with Flag-CRTH2- and Myc-GRP78-expressing plasmids.
- J Colocalization of CRTH2, LARP6, and GRP78 in NIH 3T3 cells. White arrow indicates colocalization of CRTH2, LARP6, and GRP78. Scale bar, 20 μ m.
- K Schematic diagram depicting different domains of CRTH2 involved in the interaction with LARP6 and GRP78 in the endoplasmic reticulum membrane.

Source data are available online for this figure.

revealed that ablation of CRTH2 in fibroblasts markedly exacerbated injury-induced parenchymal organ fibrosis in mice by increasing collagen synthesis, including lung (Fig 4A–E), liver (Fig 4F–J), and heart (Fig 4K–O). Given genetic ablation led to absence of CRTH2 in both plasma membrane and ER in tissues, the effect of CRTH2 in plasma membrane on organ fibrosis was not fully ruled out in mice. Genetic deletion of LARP6 (Appendix Fig S7A–D) rescued the exaggerated fibrosis in parenchymal organs in F-CRTH2 KO mice with different injuries (Fig 5A–L). Taken together, the data indicated that CRTH2 modulates collagen biosynthesis and suppresses organ fibrosis by competitive binding of mRNA-stabilized LARP6 in fibroblasts (Figs 3 and 5M).

Synthetic CRTH2 N-terminal peptide inhibits TGF- β 1-induced collagen expression in fibroblasts

We tried to interfere with LARP6-collagen mRNA binding using a synthetic CRTH2 N-terminal peptide. The TAT fragment (RKKRRQRRR) was fused to the synthetic CRTH2 polypeptide [peptide 1–36 amino acids (aa), P1–36] to facilitate cell membrane penetration (Fig EV4A). P1–36 treatment specifically reduced the binding of CRTH2 to LARP6 in a dose-dependent manner (Fig EV4B) but did not affect CRTH2 interaction with GRP78 (Fig EV4C). The inhibitory effect was not dependent on the TAT fragment (Fig EV4D). Interestingly, the P1–36 peptide treatment dramatically attenuated the elevated LARP6 binding with collagen mRNAs and collagen protein expression in TGF- β 1-challenged NIH-3T3 fibroblasts (Fig EV4E–H).

Bumetanide reduces bleomycin-induced lung fibrosis in mice by mimicking CRTH2 binding to LARP6

We then screened for potential small molecules that targeted the CRTH2 binding domain (RRM) in LARP6 protein from the large TargetMol bioactive compound library using the structure-based docking approach (Verma *et al*, 2018). After ranking, 50 compounds with top docking scores were selected for the secondary experimental screening in cultured fibroblasts (Fig 6A). As shown in Appendix Fig S8A–C, five compounds (Library code T4650, T2119, T1778, T0108, and T6088) markedly suppressed mRNA expression of Col1a1, Col1a2, and Col3a1 in TGF- β 1-treated NIH-3T3 fibroblasts. Microscale thermophoresis (MST) analysis of the five compounds (Figs EV5A–F, and 6B and C) demonstrated that T0108 (chemical name: bumetanide) had a robust physical interaction with recombinant MBP-tagged LARP6-RRM protein at an equilibrium dissociation constant (Kd) of 0.848 μ M, as compared to MBP control protein. Bumetanide directly bound to LARP6 RRM domain (Fig 6B–D) and suppressed CRTH2 N-terminal binding to LARP6 RRM domain *in vitro* (Fig 6E–F). Bumetanide treatment disrupted the LARP6-collagen mRNA complex and promoted degradation of collagen mRNA in primary fibroblasts (Fig 6G, Appendix Fig S9). These results suggested that bumetanide binds to the LARP6 RRM domain by mimicking CRTH2 in fibroblasts. We then assessed the therapeutic effects of bumetanide evident as the inhibition of pulmonary fibrosis in bleomycin-challenged mice (Fig 6H). As expected, CRTH2 deficiency in fibroblasts aggravated

Figure 3. CRTH2 deficiency increases collagen synthesis in fibroblasts through LARP6.

- A RNA immunoprecipitation and qRT-PCR (RIP-qPCR) analysis of collagen type 1, α 1 (Col1a1), collagen type 1, α 2 (Col1a2), and collagen type 3, α 1 (Col3a1) mRNA in CRTH2^{-/-} and wild-type (WT) fibroblasts using LARP6 antibody. **P* < 0.05 vs WT (two-tailed Student's *t*-test); *n* = 6 for all groups.
- B Effect of the CRTH2 deficiency on the stability of Col1a1, Col1a2, and Col3a1 mRNA in primary mouse fibroblasts. Fibroblasts were treated with 5 μ g/ml actinomycin D (Act D). Total RNA was extracted immediately after addition of Act D at 0, 2, 4, 6, 8, 12, and 24 h. Col1a1, Col1a2, and Col3a1 mRNA expression was quantitated by qRT-PCR. Dotted lines indicate mRNA half-lives; **P* < 0.05 vs WT (two-way ANOVA); *n* = 6 for all groups.
- C Effect of CRTH2 deficiency on Col1a1, Col1a2, and Col3a1 mRNA expression in primary mouse fibroblasts. GAPDH was used as housekeeping gene. **P* < 0.05 vs WT (two-tailed Student's *t*-test); *n* = 8 for all groups.
- D Effect of CRTH2 deficiency on collagen (Col) I and III protein expression in primary mouse fibroblasts with and without TGF- β 1 (10 ng/ml) treatment.
- E Knockdown efficiency of LARP6 siRNA (Si-LARP6) detected by qRT-PCR in primary fibroblasts. **P* < 0.05 vs scramble (two-tailed Student's *t*-test); *n* = 5 for all groups.
- F Effect of LARP6 knockdown on Col1a1, Col1a2, and Col3a1 mRNA stability in WT and CRTH2^{-/-} fibroblasts. **P* < 0.05 vs WT (two-way ANOVA); *n* = 8 for all groups.
- G–I Effect of LARP6 knockdown on Col1a1, Col1a2, and Col3a1 mRNA expression in WT and CRTH2^{-/-} fibroblasts. Fibroblasts were transfected with Si-LARP6 or scramble siRNA. After 48-h transfection, RNA was prepared for qRT-PCR analysis. GAPDH was used as housekeeping gene. **P* < 0.05 vs WT and #*P* < 0.05 vs scramble (two-way ANOVA); *n* = 6 for all groups.
- J Effect of LARP6 knockdown on collagen I and III protein expression in WT and CRTH2^{-/-} fibroblasts.

Data information: All data are expressed as the mean \pm standard error of the mean.

Source data are available online for this figure.

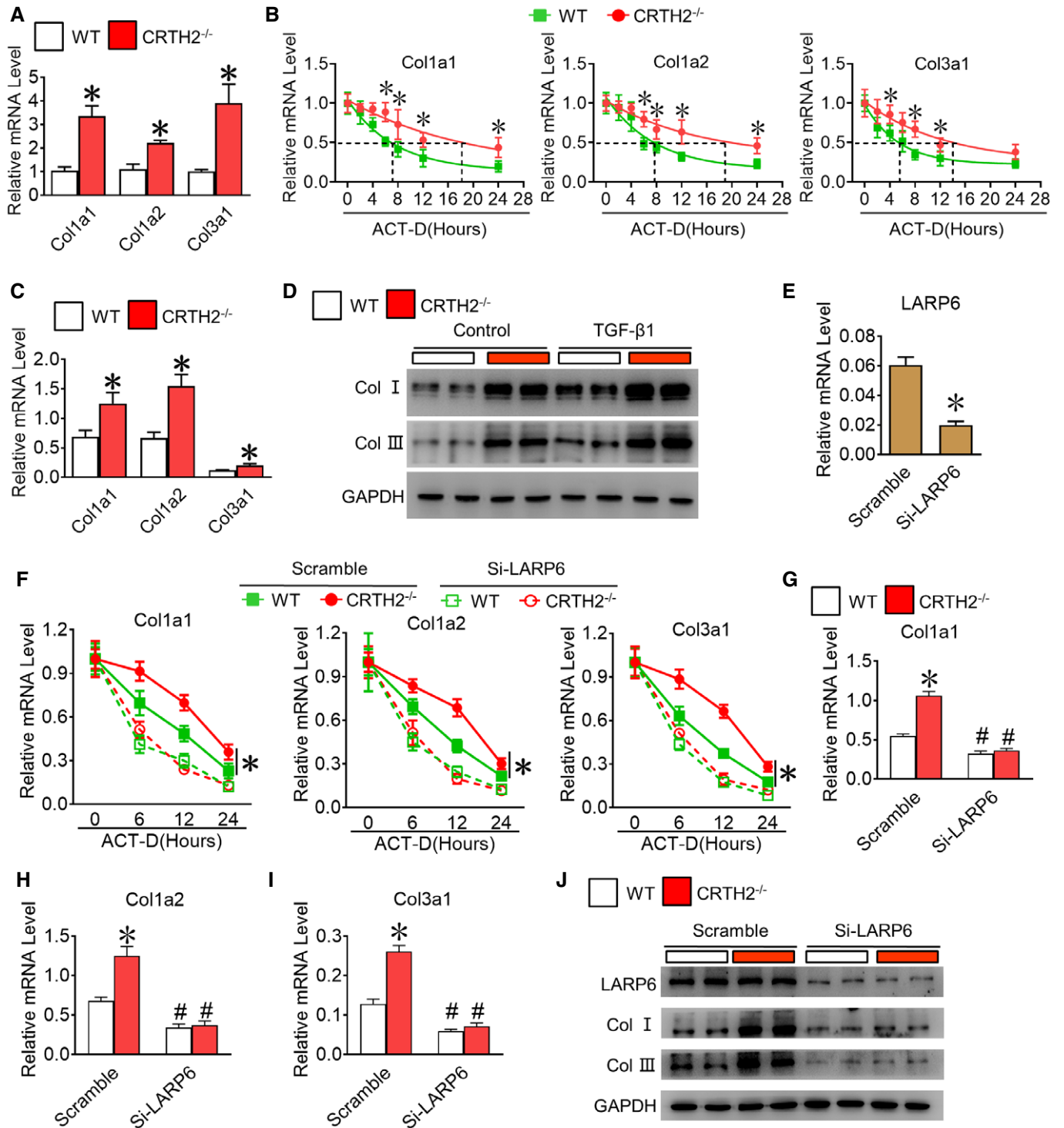


Figure 3.

bleomycin-triggered fibrosis in mice (Fig 6I–L). Bumetanide significantly relieved the bleomycin-triggered fibrosis in control mice as evidenced by reduced collagen deposition and reduced hydroxyproline component in the lungs. Bumetanide also rescued the exacerbated pulmonary fibrosis in bleomycin-challenged F-CRTH2 KO mice (Fig 6I–L).

Bumetanide reduces TGF-β1-induced collagen biosynthesis in human fibroblasts

Similarly, bumetanide treatment attenuated the interaction of CRTH2 and LARP6 in human fibroblasts MRC-5 in a dose-dependent manner (Fig 7A and B) and subsequently inhibited the binding of LARP6

with Col1a1, Col1a2, and Col3a1 mRNA in MRC-5 cells with or without TGF- β 1 challenge (Fig 7C–E). Bumetanide also suppressed the enhanced collagen mRNA and protein expression in TGF- β 1-treated MRC-5 cells (Fig 7F–I).

Discussion

CRTH2 functions as a chemoattractant receptor in cell membranes and is also involved in activation and trafficking of Th2 cells, basophils, and eosinophils to inflammatory sites (Kupczyk & Kuna, 2017). Presently, we observed CRTH2 was localized in both cytoplasmic and ER membranes in fibroblasts; caveolin-1-mediated

CRTH2 ER trafficking from plasma membrane facilitated collagen mRNA degradation through competitive binding with LARP6. Bumetanide structurally bound to the LARP6 by mimicking CRTH2 and alleviated bleomycin-triggered pulmonary fibrosis in mice. Thus, targeting CRTH2 binding to LARP6 is implicated as a promising therapeutic strategy in the treatment of organ fibrosis.

CRTH2 is a GPCR for PGD₂. CRTH2 is involved in the mediation of eosinophil activation and allergic inflammation by releasing Th2-type cytokines (Uller et al, 2007). Currently, oral competitive CRTH2 antagonists are in clinical development for the treatment of asthma (Singh et al, 2017). We observed CRTH2 was dynamically located in both cytoplasmic and ER membranes in multiple tissue fibroblasts. And the pro-fibrotic stimuli such as TGF- β 1 and PDGF-BB

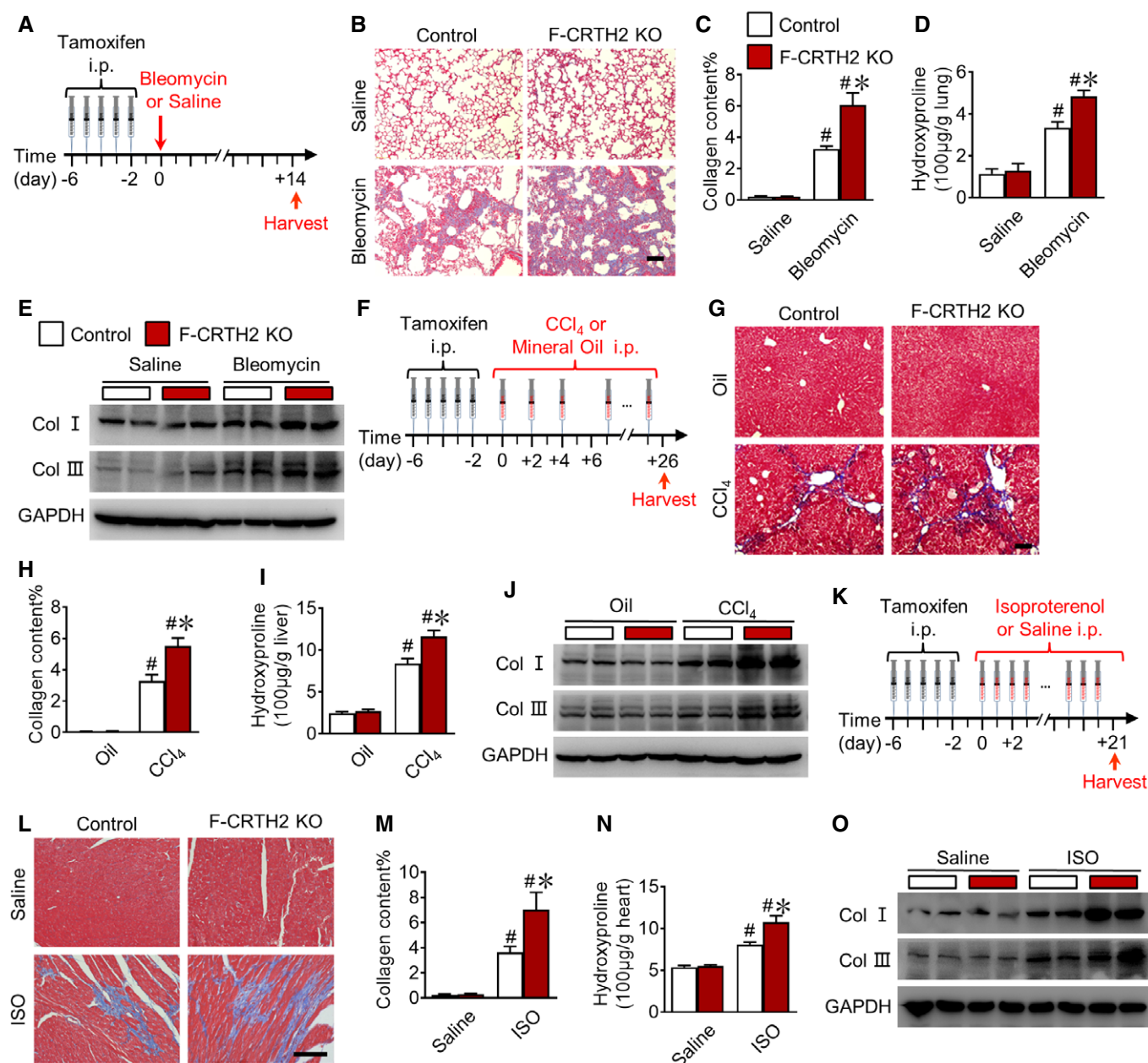


Figure 4.

Figure 4. CRTH2 deficiency in fibroblasts exacerbates injury-induced organ fibrosis in mice.

- A Schematic diagram of the bleomycin-induced lung fibrosis model in mice.
- B Representative images of Masson's trichrome staining of lung sections from CRTH2^{fllox/fllox}Col1a2-Cre^{ERT} (F-CRTH2 KO) and CRTH2^{fllox/fllox} (Control) mice 14 days after bleomycin challenge. Blue indicates the collagen deposition regions. Scale bar, 100 μ m.
- C Quantification of collagen content in mouse lung sections after bleomycin challenge. * P < 0.05 vs control and # P < 0.05 vs saline group (two-way ANOVA); saline groups, n = 4 each; and bleomycin groups, n = 8 each.
- D Hydroxyproline content in lungs from control and F-CRTH2 KO mice treated with saline or bleomycin. * P < 0.05 vs control and # P < 0.05 vs saline group (two-way ANOVA); saline groups, n = 4 each; and bleomycin groups, n = 8 each.
- E Western blot analysis of collagen (Col) I and III expression in lung tissues from control and F-CRTH2 KO mice 14 days after bleomycin challenge.
- F Protocol for CCl₄-induced liver fibrosis in mice.
- G Representative images of Masson's trichrome staining of liver sections from control and F-CRTH2 KO mice 4 weeks after CCl₄ challenge. Scale bar, 100 μ m.
- H Quantification of collagen content in mouse liver sections after CCl₄ challenge. * P < 0.05 vs control and # P < 0.05 vs mineral oil group (two-way ANOVA); mineral oil groups, n = 4 each; and CCl₄ groups, n = 8 each.
- I Hydroxyproline content in livers from control and F-CRTH2 KO mice treated with CCl₄. * P < 0.05 vs control and # P < 0.05 vs mineral oil group (two-way ANOVA); mineral oil groups, n = 4 each; and CCl₄ groups, n = 8 each.
- J Western blot analysis of collagen I and III expression in liver tissues from control and F-CRTH2 KO mice 4 weeks after CCl₄ challenge.
- K Schematic diagram of isoproterenol (ISO)-induced heart fibrosis in mice.
- L Representative images of Masson's trichrome staining of heart sections from control and F-CRTH2 KO mice 21 days after ISO challenge. Scale bar, 50 μ m.
- M Quantification of collagen content in mouse heart sections after ISO challenge. * P < 0.05 vs control and # P < 0.05 vs saline group (two-way ANOVA); PBS groups, n = 3 each; and ISO groups, n = 7-8.
- N Hydroxyproline content in hearts from control and F-CRTH2 KO mice treated with ISO. * P < 0.05 vs control and # P < 0.05 vs saline group (two-way ANOVA); saline groups, n = 4 each; and ISO groups, n = 8 each.
- O Western blot analysis of collagen I and III expression in heart tissues from control and F-CRTH2 KO mice 21 days after ISO challenge.

Data information: All data are expressed as the mean \pm standard error of the mean.
Source data are available online for this figure.

reduced CRTH2 trafficking to ER membrane, while anti-fibrotic cytokine IL-10 increased CRTH2 distribution in ER membrane. Blocking the CRTH2 trafficking to ER membrane enhanced extracellular protein biosynthesis in fibroblasts, indicating that CRTH2 membrane trafficking is essential for maintenance of extracellular matrix homeostasis. Interestingly, ER-anchored CRTH2 in fibroblasts negatively regulated cytoplasmic collagen mRNA stability by disturbing the collagen mRNA binding protein LARP6. These behaviors were not dependent on the physiological ligand PGD₂. Caveolae are flask-shaped cytoplasmic membrane structures involved in endocytosis, cholesterol and lipid metabolism, cellular signaling (Bastiani &

Parton, 2010), and GPCR trafficking (West & Hanyaloglu, 2015) that includes calcium-sensing receptor (Ray, 2015), endothelin receptor type A (Chun *et al*, 1994; Okamoto *et al*, 2000), and A1 adenosine receptor (Escrive *et al*, 2003). Caveolin-1 is the dominant component of caveolae. Caveolin-1 facilitates CRTH2 trafficking to the ER membrane. The phosphorylation of caveolin-1 on invariant serine residue 80 is required for ER retention (Schlegel *et al*, 2001). Genetic knockdown of caveolin-1 interrupts the ER retention of CRTH2 in fibroblasts, which results in increase of collagen mRNA levels in fibroblasts (Wang *et al*, 2006a). Consistent with our observations, caveolin-1 overexpression markedly ameliorates bleomycin-induced

Figure 5. LARP6 is required for deteriorated organ fibrosis in CRTH2^{-/-} mice.

- A Representative images of Masson's trichrome staining of lung sections from F-LARP6 KO and F-LARP6/F-CRTH2 double KO (F-DKO) mice 14 days after bleomycin challenge. Scale bar, 100 μ m.
- B Quantification of collagen content in mouse lung sections after bleomycin challenge. # P < 0.05 vs saline group (two-way ANOVA); saline groups, n = 4 each; and bleomycin groups, n = 7-8.
- C Hydroxyproline content in lungs from F-LARP6 KO and F-DKO mice treated with bleomycin. # P < 0.05 vs saline group (two-way ANOVA); saline groups, n = 4 each; and bleomycin groups, n = 8 each.
- D Western blot analysis of collagen (Col) I and III expression in lung tissues from F-LARP6 KO and F-DKO mice 14 days after bleomycin challenge.
- E Representative images of Masson's trichrome staining of liver sections from F-LARP6 KO and F-DKO mice 4 weeks after CCl₄ challenge. Scale bar, 100 μ m.
- F Quantification of collagen content in mouse liver sections after CCl₄ challenge. # P < 0.05 vs mineral oil group (two-way ANOVA); mineral oil groups, n = 4 each; and CCl₄ groups, n = 8 each.
- G Hydroxyproline content in livers from F-LARP6 KO and F-DKO mice treated with CCl₄. # P < 0.05 vs mineral oil group (two-way ANOVA); saline groups, n = 4 each; and CCl₄ groups, n = 8 each.
- H Western blot analysis of collagen I and III expression in liver tissues from F-LARP6 KO and F-DKO mice 4 weeks after CCl₄ challenge.
- I Representative images of Masson's trichrome staining of heart sections from F-LARP6 KO and F-DKO mice 21 days after ISO challenge. Scale bar, 50 μ m.
- J Quantification of collagen content in mouse heart sections after ISO challenge. # P < 0.05 vs saline group (two-way ANOVA); saline groups, n = 3 each; and ISO groups, n = 7 each.
- K Hydroxyproline content in hearts from F-LARP6 KO and F-DKO mice treated with ISO. # P < 0.05 vs saline group (two-way ANOVA); saline groups, n = 4 each; and ISO groups, n = 8 each.
- L Western blot analysis of collagen I and III expression in heart tissues from F-LARP6 KO and F-DKO mice 21 days after ISO challenge.
- M Schematic diagram of the working model of CRTH2-mediated collagen homeostasis in fibroblasts.

Data information: All data are expressed as the mean \pm standard error of the mean.
Source data are available online for this figure.

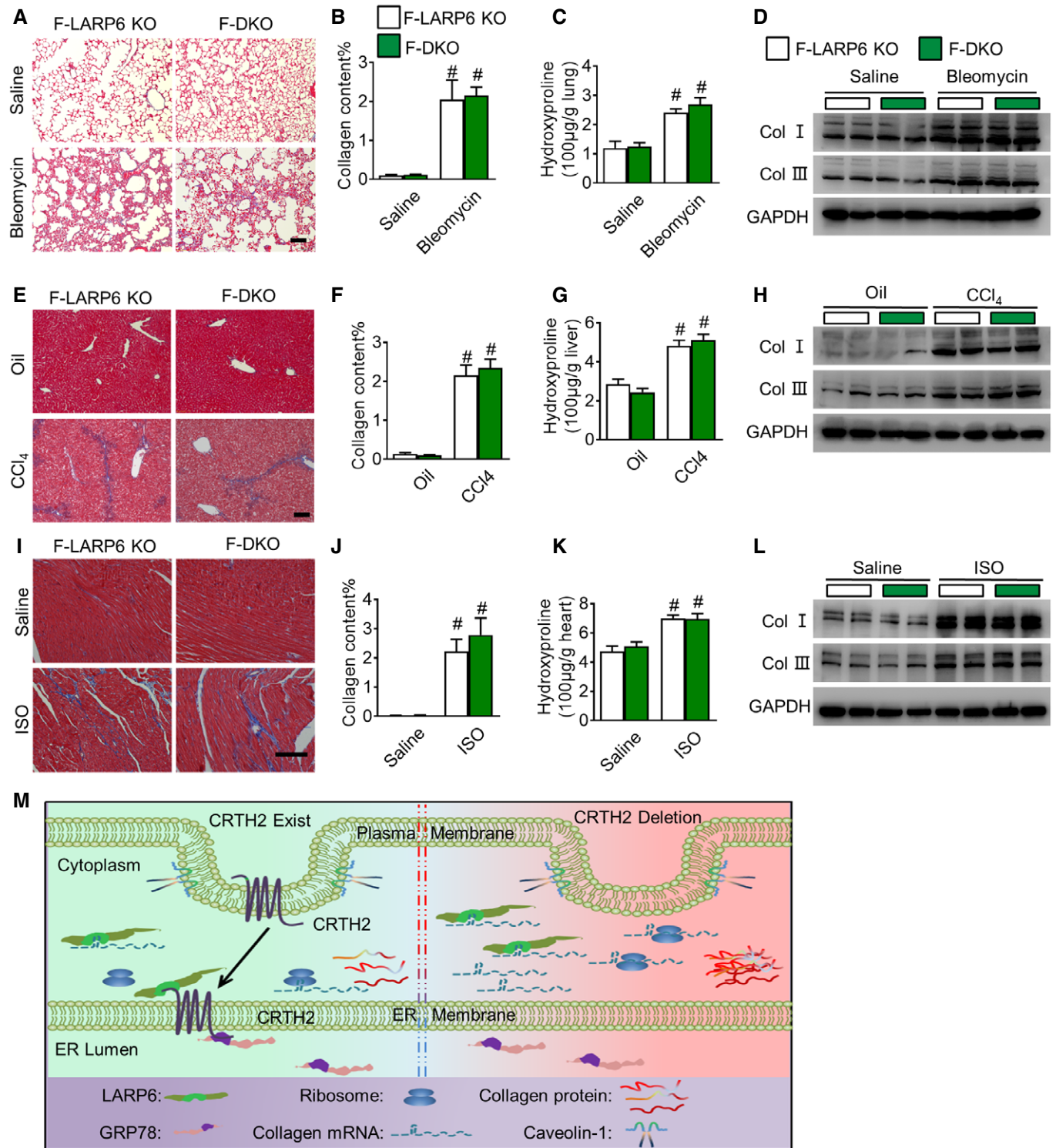


Figure 5.

pulmonary fibrosis in mice by suppressing TGF- β 1-induced ECM production (Wang *et al*, 2006b; Lin *et al*, 2019) and caveolin-1-derived peptide protects against pulmonary fibrosis (Marudamuthu *et al*, 2019). Inhibition of CRTH2-mediated Th2 activation ameliorates unilateral ureteral obstruction (UUO)-induced renal fibrosis by

secreting pro-inflammatory cytokines IL-4 and IL-13 (Ito *et al*, 2012). In contrast, global deficiency of CRTH2 aggravates bleomycin-induced pulmonary fibrosis in mice, accompanied by reduced infiltration of $\gamma\delta$ T cells in the lungs (Ueda *et al*, 2019). Moreover, protein breast regression protein-39 promotes ischemia-reperfusion injury-

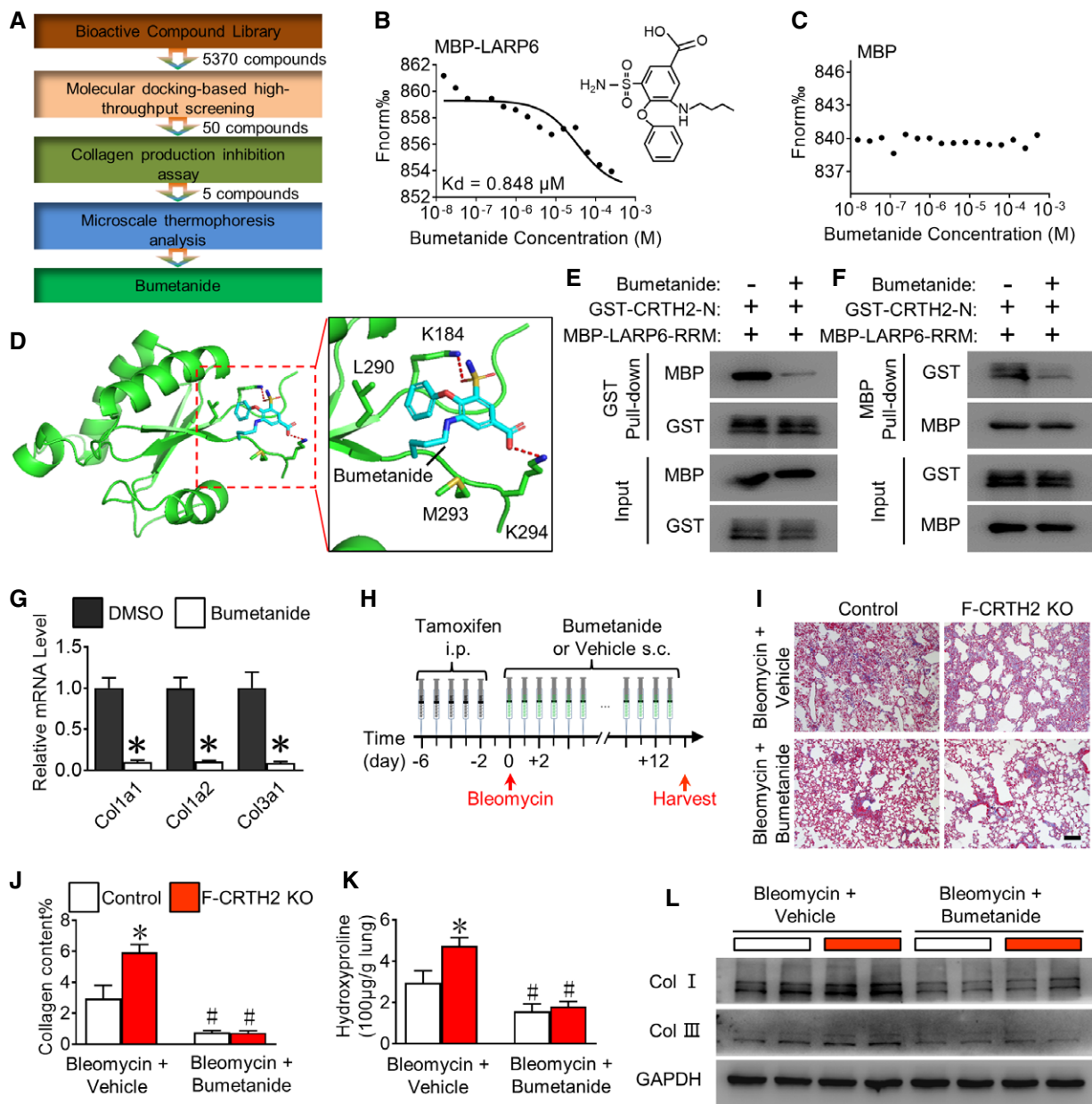


Figure 6. Bumetanide inhibits bleomycin-induced lung fibrosis in mice by targeting the LARP6 RRM domain.

- A Structure-based flow chart for the virtual screening of small molecules interacting with the LARP6-RRM domain.
- B, C Microscale thermophoresis (MST) analysis of the binding affinity of bumetanide with MBP-LARP6 and MBP control protein.
- D Binding mode of the LARP6-RRM domain with bumetanide. The protein is shown as cartoons and is green. Bumetanide and dominant residues are shown as sticks. Bumetanide is cyan, and the dominant residues are green.
- E, F Effect of bumetanide (2 μ M) on direct interaction of CRTH2 N-terminal (CRTH2-2) with LARP6 RRM domain (LARP6-4) using GST and MBP pull-down assays.
- G Effect of bumetanide on LARP6 binding to Col1a1, Col1a2, and Col3a1 mRNA in primary mouse fibroblasts. * P < 0.05 vs DMSO (unpaired two-tailed t -test); n = 6 for all groups.
- H Protocol for administration of bumetanide to bleomycin-challenged mice. Bumetanide (2 mg/kg) was subcutaneously injected in mice daily for 14 days.
- I Representative Masson's trichrome staining of lung sections from bumetanide-treated control and F-CRTH2 KO mice. Scale bars, 100 μ m.
- J Quantification of collagen content in lung sections from bumetanide-treated control (CRTH2^{fllox/fllox}) and F-CRTH2 KO mice. * P < 0.05 vs control and # P < 0.05 vs vehicle (two-way ANOVA); n = 7 for all groups.
- K Effect of bumetanide treatment on pulmonary hydroxyproline levels in control and F-CRTH2 KO mice. * P < 0.05 vs control and # P < 0.05 vs vehicle (two-way ANOVA); n = 7 for all groups.
- L Effect of bumetanide treatment on collagen (Col) I and III expression in lungs from control and F-CRTH2 KO mice.

Data information: All data are expressed as the mean \pm standard error of the mean.

Source data are available online for this figure.

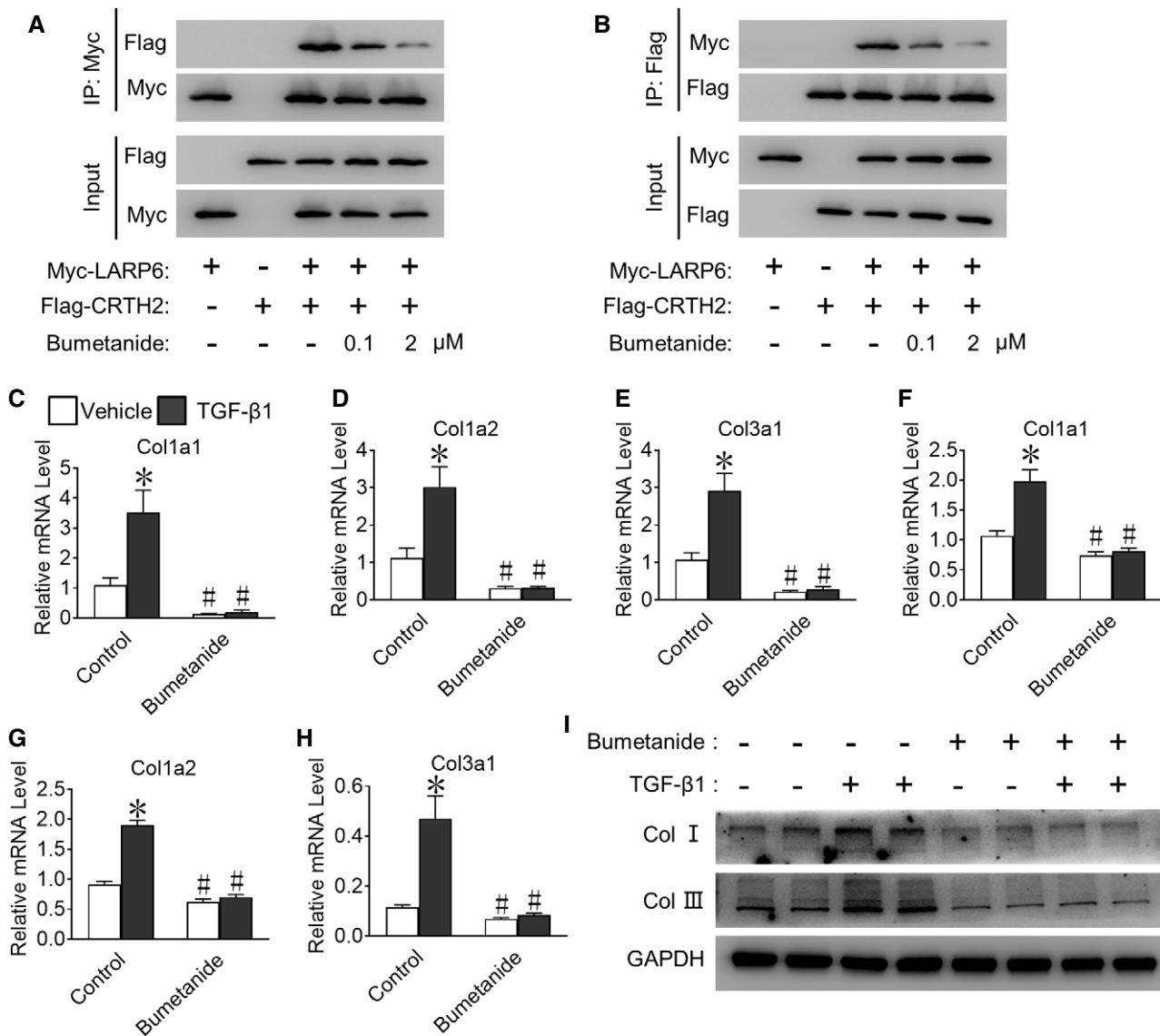


Figure 7. Bumetanide reduces TGF-β1-induced collagen biosynthesis in human fibroblasts.

A, B Bumetanide interferes with the interaction of CRTH2 with LARP6 in MRC-5 human lung fibroblasts. MRC-5 cells were co-transfected with myc-LARP6- and flag-CRTH2-expressing plasmids for 24 h and then treated with bumetanide (0.1, 2 μM) for an additional 24 h. Whole-cell lysates from MRC-5 cells were immunoprecipitated and immunoblotted with the indicated antibodies.

C–E Effect of bumetanide on LARP6 binding to Col1a1, Col1a2, and Col3a1 mRNA in cultured MRC-5 cells. MRC-5 cells were treated with TGF-β1 and bumetanide (2 μM) for 24 h. The cells were ultraviolet-cross-linked, and RNA-bound proteins were immunoprecipitated with LARP6 antibody followed by RNA extraction for qRT-PCR. * $P < 0.05$ vs vehicle and # $P < 0.05$ vs control (two-way ANOVA); $n = 6$ for all groups.

F–H Effect of bumetanide on Col1a1, Col1a2, and Col3a1 mRNA expression in MRC-5 cells. GAPDH was used as housekeeping gene. * $P < 0.05$ vs vehicle and # $P < 0.05$ vs control (two-way ANOVA); $n = 6$ for all groups.

I Effect of bumetanide on collagen (Col) I and III protein expression in MRC-5 cells.

Data information: All data are expressed as the mean ± standard error of the mean.

Source data are available online for this figure.

induced renal fibrosis by acting on membrane CRTH2 in macrophages, but not in fibroblasts (Montgomery *et al.*, 2017). These observations indicate that CRTH2 in inflammatory cells may function differently in organ fibrogenesis.

Collagen, especially type I, is the major component in the ECM in fibrotic organs (Herrera *et al.*, 2018). In eukaryotic cells, collagen

synthesis process is precisely regulated at multiple levels that include mRNA transcription, mRNA stability, post-translational modifications of protein, and protein maturation and degradation (Zhang & Stefanovic, 2016b). The exacerbated collagen deposition during organ fibrosis seems to be mainly due to the increased stability of collagen mRNAs and their translation (Lindquist *et al.*, 2000;

Zhang & Stefanovic, 2016b). LARP6 binds an evolutionally conserved 5' stem-loop structure of type I and III collagen mRNAs to preserve their stability and translatability through the N-terminal RRM domain (Cai *et al*, 2010a). Moreover, interaction of LARP6 with vimentin (Challa & Stefanovic, 2011) and non-muscle myosin (Cai *et al*, 2010b) facilitates binding to collagen mRNAs and partitioning of collagen mRNAs from the ER membrane, respectively. We observed myosin in the LARP6 and CRTH2 protein complex in fibroblasts (Fig 2A). ER-anchored CRTH2 inhibited the binding of LARP6 to collagen mRNAs and their subsequent translation to maintain collagen homeostasis in tissues. Silencing GRP78 did not influence the ER distribution of CRTH2 and collagen synthesis in fibroblasts, indicating GRP78 may serve as one of non-functional structural proteins in ER. Indeed, other ER chaperone proteins such as CKAP4, TGM2, and TERA (Fujita *et al*, 2013; Harada *et al*, 2020; Lee *et al*, 2021) were also detected in co-immunoprecipitations of CRTH2 by mass spectrometry (data not shown). CRTH2-derived small peptide or small molecules mimicking CRTH2 binding to LARP6 markedly reduced collagen mRNA stability and expression in fibroblasts. Therefore, CRTH2 in the ER membrane functions as a scaffold protein to regulate collagen biosynthesis by binding to LARP6. Targeting ER CRTH2-LARP6 binding may serve as a therapeutic strategy for organ fibrosis.

Among 5370 bioactive compounds, through computational docking and an *in vitro* binding assay we identified three small molecule chemicals C188-9 (STAT-3 inhibitor), venetoclax (Bcl-2 inhibitor), and bumetanide (Na-K-2Cl cotransporter isoform 1 inhibitor), which directly bind LARP6 as CRTH2. The three compounds suppressed TGF- β 1-evoked collagen expression in fibroblasts. STAT-3 activation integrates a common pro-fibrotic pathway to promote tissue fibrosis (Chakraborty *et al*, 2017). C188-9 ameliorates the progression of pulmonary and skin fibrosis in mice exposed to bleomycin (Kasembeli *et al*, 2018; Pedroza *et al*, 2018). Likewise, Bcl2 is involved in tissue fibrosis (Safaeian *et al*, 2014; Weder *et al*, 2018). Thus, C188-9 and venetoclax show promising anti-fibrotic activity by targeting multiple pathways. Bumetanide is an older diuretic medication used to treat fluid retention caused by congestive heart failure and hepatic and renal disease (Edwards & Crambert, 2017). We found bumetanide treatment notably suppressed the development of bleomycin-induced lung fibrosis in mice and reduced collagen expression in human fibroblasts. These observations warrant further investigation concerning the clinical application of bumetanide for patients with fibrotic diseases.

In this study, we identified that the ER-anchored CRTH2 regulated collagen mRNA stability in fibroblasts by interacting with LARP6, and bumetanide suppressed collagen biosynthesis in fibroblasts by mimicking CRTH2 binding to LARP6. Targeting the interaction of CRTH2 with LARP6 might be a promising therapeutic approach for the treatment of organ fibrosis.

Materials and Methods

Animals

All animals were maintained in a C57/BL6 background in accordance with the guidelines of the Institutional Animal Care and Use Committee of the Tianjin Medical University. Mice were housed in a

dedicated animal facility with a controlled temperature of 25°C and a light-controlled, 12-h light/dark cycle. HA-CRTH2 mice were generated using CRISPR/Cas9 strategy by the Center for Excellence in Molecular Cell Science of Chinese Academy of Sciences (Shanghai, China) (Tao *et al*, 2021). CRTH2^{flox/flox} or LARP6^{flox/flox} mice were bred with Col1a2-Cre^{ERT} mice to generate fibroblast-specific CRTH2 (F-CRTH2) or LARP6 (F-LARP6) KO mice, respectively. Mice were intraperitoneally injected with tamoxifen (75 mg/kg body-weight, 20 mg/ml in corn oil) for 5 consecutive days at 5–7 weeks of age (Li *et al*, 2017). For mouse genotyping, genomic DNA prepared from tail specimens 2 weeks after birth was used for standard PCR assays. The detailed primer sequences are listed in Appendix Table S1.

Reagents

Recombinant human TGF- β 1 and PDGF-BB were purchased from R&D Systems (Minneapolis, MN, USA). DK-PGD₂ and CAY10595 were obtained from Cayman Chemical (Ann Arbor, MI, USA). Recombinant mouse IL-4, IL-10, and anti-IFN γ were purchased from BiLegend (San Diego, CA, USA). Bleomycin sulfate and genistein were purchased from Selleck Chemicals (Houston, TX, USA). CCl₄ (>99.0% purity) was purchased from Aladdin Technologies Inc. (Shanghai, China). Actinomycin D, sucrose, and isoproterenol (ISO) were obtained from Sigma-Aldrich (St. Louis, MO, USA). The bioactive compound library was obtained from TargetMol (Wellesley Hills, MA, USA).

Cell line culture, treatment, and transfection

HEK293T, vascular smooth muscle cells (VSMCs), HeLa, MRC-5, and NIH 3T3 cells were purchased from Cell Bank (Shanghai Institutes for Biological Sciences, Shanghai, China). VSMCs were grown in complete medium (DMEM/F-12; Gibco, Carlsbad, CA, USA; 12634010) supplemented with 10% (vol/vol) fetal bovine serum (FBS; Gibco, 10099141) and 50 μ g/ml penicillin/streptomycin (Gibco, 15070063). Other cells were cultured in DMEM (Gibco, 11965092) with 50 μ g/ml penicillin/streptomycin and 10% (vol/vol) FBS.

Fibroblasts were treated with TGF- β 1 (10 ng/ml) or actinomycin D (5 μ g/ml) for the indicated times for induction of collagen expression and assessment of mRNA decay, respectively. Cells were cultured in serum-free medium before transfection, and recombinant DNA plasmids were transfected into cells using Lipofectamine 2000 (Thermo Fisher Scientific, Waltham, MA, USA). Approximately 1 μ g of plasmid and 2.5 μ l of Lipofectamine 2000 were separately added into 250 μ l of serum-free DMEM for 5 min. The mixture was put into the cell dish. After 6 h, the medium was changed to complete medium. Cells were used for protein extraction or immunostaining at indicated times. All cell lines tested negative for mycoplasma.

Plasmids

The mouse CRTH2, LARP6, GRP78, and caveolin-1 genes with or without Flag, GST, green fluorescent protein (GFP), Myc, and Flag-SBP tags were cloned into the pRK5 vector using Sal I and Not I restriction enzymes from cDNA. For prokaryotic expression plasmids, CRTH2-2 (1-36 aa), CRTH2-4 (306-382 aa), LARP6-4 (180-299

aa), and MBP-GRP78-4 (390–510 aa) were inserted into the pGEX-4T-3 or pMAL-C2X vector using PCR.

Confocal calcium imaging

Ca²⁺ transients were recorded in NIH 3T3 cells using a laser-scanning confocal microscope (Carl Zeiss, Inc., Germany) (Shen *et al*, 2016). Briefly, cells were loaded with 6 µg/ml Fluo-3 (Dojindo Laboratories, Kumamoto, Japan) in Hank's balanced salt solution (Invitrogen, Carlsbad, CA, USA.) for 30 min at 37°C. Ca²⁺ flux was evaluated by rapid application of DK-PGD₂ after treatment of genistein or CAY10595. Fluo-3 was excited at 488 nm. Images were acquired in the line-scan (X-T) mode with 512 pixels per line at a rate of 5 ms per scan, and the change of fluorescence intensity was recorded.

Mouse fibrocyte preparation

Mouse fibrocytes were harvested and cultured as previously described (Phillips *et al*, 2004; Ozono *et al*, 2021). Briefly, mononuclear cells were isolated by Lympholyte-Mammal (Cedarlane, Burlington, NC, USA) from bone marrow cells and then cultured in DMEM supplemented with 20% FCS, penicillin, streptomycin, and L-glutamine for 6 days. This crude cell preparation contaminating with B cells, T cells, and monocytes/macrophages was purified by magnetic immunodepletion using anti-CD19, anti-CD14, and anti-CD3, respectively (DynaL Inc., Lake Success, New York, USA). The purified fibrocytes were returned to culture for an additional 5 days before analysis. Fibrocytes more than 90% purity as determined by flow cytometry CD45⁺/collagen-1⁺/CXCR4⁺ (anti-mouse PE-Cyanine7-CD45; PE-CXCR4; anti-mouse biotin-collagen-1+anti-biotin FITC, eBioscience, California, USA) were used for further analysis.

Small interfering RNA (siRNA) transfection

The siRNA for caveolin-1, β-arrestin-1, β-arrestin-2, LARP6, and GRP78, and Scramble siRNA were purchased from GenePharma (Shanghai, China). The siRNA sequences are listed in Appendix Table S2. The siRNAs were transfected into NIH 3T3 cells or primary fibroblasts using Lipofectamine 2000 according to the manufacturer's instructions. At 24 h or indicated times after the transfection, cells were collected for further analysis.

Mouse primary fibroblast culture

Primary lung fibroblasts were isolated and cultured as previously described (Tager *et al*, 2008). Lung tissues were removed from anesthetized mice, cut into small pieces, and digested in enzymatic digestion buffer (1% collagenase type III, 0.125% trypsin, and DNase I in DMEM) for 90 min at 37°C while shaking slightly. Primary murine lung fibroblasts were grown at 37°C in a 5% CO₂ atmosphere in DMEM supplemented with 10% FBS and 1% penicillin/streptomycin. Lung fibroblasts were used between passages 3 to 6.

Experimental organ fibrosis

Pulmonary fibrosis was induced in mice using bleomycin as previously described (Li *et al*, 2011). Briefly, 7- to 8-week-old male mice

were anesthetized with isoflurane. Bleomycin (3.5 mg/kg in 50 µl 0.9% sterile saline) or vehicle (0.9% sterile saline) was instilled intratracheally into mice. The mice were sacrificed after 14 days of instillation, and lungs were removed for histological analysis.

Cardiac fibrosis was induced in mice by the administration of ISO as previously described (Acin-Perez *et al*, 2018). Briefly, 6- to 8-week-old male mice were subcutaneously injected with ISO (10 mg/kg/day) for 21 consecutive days under isoflurane anesthesia. A matched group of control mice were injected with PBS. Mice were sacrificed, and hearts were harvested 21 days after ISO treatment.

Live fibrosis was induced in by CCl₄ treatment (Saijou *et al*, 2018). Briefly, 6- to 8-week-old male mice were given intraperitoneal injections with CCl₄ (1 µl/g body weight, diluted 1:1 in mineral oil) three times weekly for 4 weeks. An equal volume of mineral oil was administered to control animals. Livers were harvested one day after the final CCl₄ injection.

Histological analysis

Excised lungs, hearts, and livers were fixed with 4% buffered paraformaldehyde, paraffin-embedded, and serially sectioned at 5 µm thickness. Masson's trichrome was applied according to the manufacturer's instructions (Sigma-Aldrich, HT15-1KT). For the evaluation of tissue fibrosis, photographs of at least five different light microscopy fields per section were taken using a digital camera (Leica Microsystems, Wetzlar, Germany). IPP software was used to analyze the collagen density as previously described (Tang *et al*, 2017).

RNA immunoprecipitation (RIP)

RIP was performed as previously described (Li *et al*, 2017) with some modifications. Briefly, cells were seeded in 10-cm dish and grown to 90% confluency. The cells were cross-linked by irradiation with 400 mJ/cm² ultraviolet light for 5 min before trypsin digestion. Cells were collected by centrifugation (5 min, 1,000 g, 4°C) and lysed in ice-cold RIP buffer (0.1% sodium dodecyl sulfate [SDS], 0.5% NP-40, 0.5% sodium deoxycholate, and 10% glycerol in PBS) containing 200 U/ml RNase inhibitor (TaKaRa Bio, Shiga, Japan) and 1% protease inhibitor cocktail (TargetMol) on ice for 15 min. Cell lysates were centrifuged at 16,000 g for 20 min at 4°C, followed by addition of 40 U RQ1 RNase-free DNase (Promega, Madison, WI, USA) to digest DNA at 37°C for 10 min. The supernatant was incubated with LARP6 antibody or control IgG overnight at 4°C. The immunoprecipitates were further incubated with protein A or G beads (Beyotime, Shanghai, China) for 3 h at 4°C. The beads were washed five times with cold RIP buffer and resuspended in 1 ml TRIzol (Invitrogen). RNAs were extracted and analyzed using qRT-PCR.

Immunofluorescence staining

Cells were cultured on glass coverslips (BD Biosciences, Santa Clara, CA, USA) in a 12-well plate and transfected with the cDNA-expressing plasmids using Lipofectamine 2000 (Thermo Fisher Scientific) for 48 h. The cells were fixed in 4% paraformaldehyde for 10 min, washed three times with PBS, then permeabilized, and blocked using 3% bovine serum albumin in PBS containing 0.1% Triton X-100 for 45 min at room temperature. Cells were incubated with antibody to myc, LARP6, and GRP78 (all 1:100; Abclonal

Technology, Woburn, MA, USA), anti-Calnexin (1:100; Abcam, Cambridge, UK), and anti-GFP (1:500; Invitrogen) antibodies overnight at 4°C. After washing three times with PBS, the cells were incubated with Alexa Fluor 594-conjugated anti-mouse IgG, Alexa Fluor 647-conjugated anti-mouse IgG, or Alexa Fluor 488-conjugated anti-rabbit IgG antibody (1:1,000; Invitrogen) for 2 h. The slides were mounted in ProLong Gold antifade reagent with 4',6-diamidino-2-phenylindole (DAPI; Invitrogen). All immunofluorescence pictures were captured and analyzed using a laser-scanning confocal microscope (Carl Zeiss, Oberkochen, Germany). At least five random fields were examined for each glass slide. Colocalization was quantified by calculating fluorescence intensity correlation coefficient value using the count and measure objects plugin feature of Image-Pro Plus (Media Cybernetics, Rockville, MD, USA).

Purification of membrane and lipid raft protein

Plasma and ER membrane proteins were isolated from NIH 3T3 cells using a plasma and ER membrane protein extraction kit (BestBio, Shanghai, China). Lipid raft fractions were purified from NIH 3T3 cells using a modified sucrose density gradient ultracentrifugation method (Zhu *et al.*, 2000). Briefly, four 10-cm dishes containing cultured NIH 3T3 cells were transfected with Myc-CRTH2. Forty-eight hours after the transfection, the cells were placed on ice and washed twice with PBS. The washed cells were harvested in 1.2 ml MBS buffer [25 mM 2-(N-morpholino) ethanesulfonic acid, 4-morpholineethanesulfonic acid; (Sigma-Aldrich), 150 mM NaCl, pH 6.5, and protease inhibitor cocktail] and homogenized by passing 15 times through a 25-gauge needle attached to a 1-ml syringe, followed by three applications of a high power ultrasonic cell disruptor. The homogenized sample (1.6 ml) was mixed with 1.6 ml 90% sucrose/MBS and loaded in a centrifuge tube (Beckman Instruments, Brea, CA, USA) by overlaying with 3.2 ml of 35% sucrose and 3.2 ml of 5% sucrose. The gradients were centrifuged at 260,000 g using a SW40Ti rotor (Beckman Instruments) for 18 h. A total of 12 fractions (800 µl per fraction) were carefully collected from the top to the bottom of the gradient. The composition of each fraction was determined by Western blot.

Protein purification

Proteins were expressed in BL21 codon plus bacteria (Stratagene, San Diego, CA, USA) and purified as described previously (Wang *et al.*, 2018). Briefly, pMAL-C2X (MBP tag) and pGEX-4T-3 (GST tag) vectors expressing different truncated proteins were transformed into BL21 codon plus bacteria. Protein expression was induced by addition of 0.5 mM isopropyl β-d-1-thiogalactopyranoside for 24 h at 16°C. Bacterial cell pellets were resuspended in cold PBS containing 5 mM 2-mercaptoethanol, 1% Triton X-100, 1 mM phenylmethylsulfonyl fluoride, and 2 mM EDTA and extensively ultrasonicated. GST-recombinant proteins and MBP-tagged proteins were purified following the protocol of the manufacturer (GenScript, Zhenjiang, China).

Western blot analysis

Tissue protein was extracted in the lysis buffer with protease inhibitors. The protein concentrations were determined using a BCA

Protein Assay Kit (Pierce, Rockford, IL, USA). Equivalent levels of proteins were denatured and resolved by 10% SDS-polyacrylamide gel electrophoresis (SDS-PAGE) and transferred to nitrocellulose membranes. Each membrane was incubated with 5% skimmed milk and probed with primary antibodies overnight at 4°C. Primary antibodies and dilutions used were as follows: anti-calnexin (1:1,000; Abcam), anti-caveolin-1 (1:200; Santa Cruz Biotechnology, Dallas, TX, USA), anti-collagen I and anti-collagen III (1:1,000; Proteintech Group, Rosemont, IL, USA), anti-glyceraldehyde-3-phosphate dehydrogenase (GAPDH, 1:10,000; Proteintech Group), and anti-ATP1B, anti-LARP6, anti-Flag, anti-Myc, anti-HA, and anti-GST (all 1:1,000; Abclonal Technology). The membranes were washed and then incubated with horseradish peroxidase-labeled secondary antibody for 1–2 h at room temperature. Proteins were visualized using an enhanced chemiluminescence reagent (Thermo Fisher Scientific). The relative protein densitometry was quantified using ImageJ 1.44 software (NIH, Bethesda, MD, USA).

Silver staining and mass spectrometry

Lysates from NIH 3T3 stable cell lines stably expressing myc-CRTH2 were prepared using lysis buffer containing protease inhibitor cocktail (Roche, Basel, Switzerland). Myc-tagged protein complexes in the cell lysates were captured by incubation with anti-myc magnetic beads (Sigma-Aldrich). After binding, the beads were washed five times with ice-cold PBS plus 0.1% NP-40. Myc peptide was applied to elute the myc-protein complexes from the beads. The eluted complexes were added 6× SDS loading buffer and boiled for 10 min at 95°C. The proteins in the samples were separated by 10% SDS-PAGE, and the gels were silver-stained using a commercial kit (Beyotime, Shanghai, China). Bands of interest were excised and examined using nano-liquid chromatography coupled to a Q-Exactive mass spectrometer (Thermo Fisher Scientific).

Quantitative real-time polymerase chain reaction (RT-PCR) and mRNA half-life

Total RNA from the NIH 3T3 cells or primary fibroblasts was extracted using TRIzol reagent (Life Technologies, Carlsbad, CA, USA) according to the manufacturer's instructions. Total RNA (1 µg) was reverse-transcribed to cDNA using a Reverse Transcription Reagent kit (TaKaRa Bio) according to the manufacturer's method. Target gene expression was normalized to the level of *gapdh* mRNA. The RT-PCR protocol comprised 5 min at 95°C for one cycle, followed by 40 cycles at 95°C for 30 s, 60°C for 30 s, and 72°C for 20 s, and a final extension at 72°C for 10 min. Relative transcript level of a gene is expressed in ΔCt values ($\Delta C_t = C_{t \text{ reference}} - C_{t \text{ target}}$). Relative changes in transcript levels compared with controls are expressed as ΔΔCt values ($\Delta\Delta C_t = \Delta C_t \text{ treated} - \Delta C_t \text{ control}$), as previously described (Lagares *et al.*, 2017). All the primer sequences are listed in Appendix Table S3. For mRNA half-life measurements, actinomycin D (ActD, 5 µg/ml; Sigma) was added to the cells for 1, 2, 4, 6, 8, 12, and 24 h prior to extraction of total RNA. The mRNA half-life determinations were deduced by the one-phase exponential decay method (Al-Saif & Khabar, 2012) using GraphPad Prism software (GraphPad Software, San Diego, CA).

In vitro binding assays

The binding affinity of LARP6 to compounds was determined by microscale thermophoresis (MST). Briefly, the recombinant MBP-LARP6 protein or MBP control protein was purified using the AKTA Fast Protein Liquid Chromatography system, and the buffer was exchanged with 20 mM HEPES (pH 7.5) and 100 mM NaCl. MBP-LARP6 protein and MBP control protein were fluorescently labeled using the NT 647-labeling kit (NanoTemper Technologies, München, Germany). The assays were performed in buffer containing 20 mM HEPES (pH 7.5), 100 mM NaCl, and 0.05% Tween-20. After a short incubation, the samples were loaded into MST NT.115 standard glass capillaries. Prior to each experiment, it was confirmed that no sample was adherent to the capillary walls and no sample aggregation had occurred. Labeled MBP-LARP6 protein was incubated at a constant concentration (1 μ M), while the concentration of ligand (different compounds) was twofold serially diluted to 16 different concentrations (from 1 μ M to 0.03 nM). Sixteen titration series of ligand were mixed with labeled MBP-LARP6 to produce the final reaction mix. Fluorescence was analyzed in the Monolith NT.115 device (NanoTemper Technologies, München, Germany). The MST power and excitation power were 20 and 75%, respectively. The measurement protocol was as follows: fluorescence before 5 s, MST for 20 s, fluorescence after 5 s, and a delay of 25 s. The K_d values were calculated by the NT Analysis software (NanoTemper Technologies).

Statistical analyses

All data are expressed as the mean \pm standard error of the mean. Statistical analysis was performed using GraphPad Prism 8 (GraphPad Software, Inc., San Diego, CA, USA) and Statistical Package for the Social Sciences (SPSS, IBM Corp, Armonk, NY, USA). The data normal distribution was examined using Shapiro–Wilk normality test. Comparisons between two groups were assessed by using the Mann–Whitney U-test or the two-tailed Student's *t*-test. Multiple group analyses were compared with one- or two-way analysis of variance (ANOVA) with Bonferroni post-tests. In all experiments, *P*-values < 0.05 were considered statistically significant.

Data availability

The raw mass spectrometry proteomics data have been deposited to the ProteomeXchange Consortium via the iProX partner repository with the dataset identifier PXD025610 (<http://proteomecentral.proteomexchange.org/cgi/GetDataset?ID=PX025610>). The original immunoblots and gels are provided in the source data file. Primer and siRNA sequence used in this study are listed in Appendix Tables S1–S3. This study includes no data deposited in external repositories.

Expanded View for this article is available online.

Acknowledgments

This work was supported by the National Natural Science Foundation of China (81790623, 82030015, 31800995, 31771269, 81970540), the Chinese Ministry of Science and Technology (2017YFC1307404, 2018YFA0800601), the China Postdoctoral Science Foundation (2018M640242), the National Postdoctoral

Program for Innovative Talents (BX20180215), and the Natural Science Foundation of Tianjin (17JCQJC45700). Dr. Yu is a fellow at the Jiangsu Collaborative Innovation Center for Cardiovascular Disease Translational Medicine.

Author contributions

SZ, YS, and YY designed the study. SZ performed most of the experiments. JL, BW, and DK conducted some animal experiments. HC, YJ, and LY performed the compound screening and docking experiments. CW, XX, GC, YW, KZ, YS, JD, and DA. provided the experimental assistance. SZ, YS, and YY analyzed the data. SZ, YS, and YY wrote the paper.

Conflict of interest

The authors declare that they have no conflict of interest.

References

- Acin-Perez R, Lechuga-Vieco AV, Del Mar MM, Nieto-Arellano R, Torroja C, Sanchez-Cabo F, Jimenez C, Gonzalez-Guerra A, Carrascoso I, Benincá C *et al* (2018) Ablation of the stress protease OMA1 protects against heart failure in mice. *Sci Transl Med* 10: eaan4935
- Al-Saif M, Khabar KSA (2012) UU/UA dinucleotide frequency reduction in coding regions results in increased mRNA stability and protein expression. *Mol Ther* 20: 954–959
- Bastiani M, Parton RG (2010) Caveolae at a glance. *J Cell Sci* 123: 3831–3836
- Busija AR, Patel HH, Insel PA (2017) Caveolins and cavins in the trafficking, maturation, and degradation of caveolae: implications for cell physiology. *Am J Physiol Cell Physiol* 312: C459–C477
- Cai L, Fritz D, Stefanovic L, Stefanovic B (2010a) Binding of LARP6 to the conserved 5' stem-loop regulates translation of mRNAs encoding type I collagen. *J Mol Biol* 395: 309–326
- Cai L, Fritz D, Stefanovic L, Stefanovic B (2010b) Nonmuscle myosin-dependent synthesis of type I collagen. *J Mol Biol* 401: 564–578
- Chakraborty D, Sumova B, Mallano T, Chen CW, Distler A, Bergmann C, Ludolph I, Horch RE, Gelse K, Ramming A *et al* (2017) Activation of STAT3 integrates common profibrotic pathways to promote fibroblast activation and tissue fibrosis. *Nat Commun* 8: 1130
- Challa AA, Stefanovic B (2011) A novel role of vimentin filaments: binding and stabilization of collagen mRNAs. *Mol Cell Biol* 31: 3773–3789
- Chun M, Liyanage UK, Lisanti MP, Lodish HF (1994) Signal transduction of a G protein-coupled receptor in caveolae: colocalization of endothelin and its receptor with caveolin. *Proc Natl Acad Sci USA* 91: 11728–11732
- Edwards A, Crambert G (2017) Versatility of NaCl transport mechanisms in the cortical collecting duct. *Am J Physiol-Renal* 313: F1254–F1263
- Escrive M, Burgueno J, Ciruela F, Canela EI, Mallol J, Enrich C, Lluís C, Franco R (2003) Ligand-induced caveolae-mediated internalization of A1 adenosine receptors: morphological evidence of endosomal sorting and receptor recycling. *Exp Cell Res* 285: 72–90
- Fujita K, Nakamura Y, Oka T, Ito H, Tamura T, Tagawa K, Sasabe T, Katsuta A, Motoki K, Shiwaku H *et al* (2013) A functional deficiency of TERA/VCP/p97 contributes to impaired DNA repair in multiple polyglutamine diseases. *Nat Commun* 4: 1816
- Harada T, Sada R, Osugi Y, Matsumoto S, Matsuda T, Hayashi-Nishino M, Nagai T, Harada A, Kikuchi A (2020) Palmitoylated CKAP4 regulates mitochondrial functions through an interaction with VDAC2 at ER-mitochondria contact sites. *J Cell Sci* 133: jcs249045
- Herrera J, Henke CA, Bitterman PB (2018) Extracellular matrix as a driver of progressive fibrosis. *J Clin Invest* 128: 45–53

- Hirai H, Tanaka K, Yoshie O, Ogawa K, Kenmotsu K, Takamori Y, Ichimasa M, Sugamura K, Nakamura M, Takano S et al (2001) Prostaglandin D2 selectively induces chemotaxis in T helper type 2 cells, eosinophils, and basophils via seven-transmembrane receptor CRTH2. *J Exp Med* 193: 255–261
- Ito H, Yan X, Nagata N, Aritake K, Katsumata Y, Matsuhashi T, Nakamura M, Hirai H, Urade Y, Asano K et al (2012) PGD2-CRTH2 pathway promotes tubulointerstitial fibrosis. *J Am Soc Nephrol* 23: 1797–1809
- Kasembeli MM, Bharadwaj U, Robinson P, Tweardy DJ (2018) Contribution of STAT3 to inflammatory and fibrotic diseases and prospects for its targeting for treatment. *Int J Mol Sci* 19: 2299
- Kendall RT, Feghali-Bostwick CA (2014) Fibroblasts in fibrosis: novel roles and mediators. *Front Pharmacol* 5: 123
- Kupczyk M, Kuna P (2017) Targeting the PGD2/CRTH2/DP1 signaling pathway in asthma and allergic disease: current status and future perspectives. *Drugs* 77: 1281–1294
- Lagares D, Ghassemi-Kakroodi P, Tremblay C, Santos A, Probst CK, Franklin A, Santos DM, Grasberger P, Ahluwalia N, Montesi SB et al (2017) ADAM10-mediated ephrin-B2 shedding promotes myofibroblast activation and organ fibrosis. *Nat Med* 23: 1405–1415
- Leask A (2010) Potential therapeutic targets for cardiac fibrosis TGF beta, angiotensin, endothelin, CCN2, and PDGF, partners in fibroblast activation. *Circ Res* 106: 1675–1680
- Lee HJ, Jung YH, Choi GE, Kim JS, Chae CW, Lim JR, Kim SY, Yoon JH, Cho JH, Lee SJ et al (2021) Urolithin A suppresses high glucose-induced neuronal amyloidogenesis by modulating TGM2-dependent ER-mitochondria contacts and calcium homeostasis. *Cell Death Differ* 28: 184–202
- Li W, Zhang Z, Liu X, Cheng X, Zhang Y, Han X, Zhang Y, Liu S, Yang J, Xu B et al (2017) The FOXN3-NEAT1-SIN3A repressor complex promotes progression of hormonally responsive breast cancer. *J Clin Invest* 127: 3421–3440
- Li Y, Jiang D, Liang J, Meltzer EB, Gray A, Miura R, Wogensen L, Yamaguchi Y, Noble PW (2011) Severe lung fibrosis requires an invasive fibroblast phenotype regulated by hyaluronan and CD44. *J Exp Med* 208: 1459–1471
- Li Y, Li Z, Zhang C, Li P, Wu Y, Wang C, Bond Lau W, Ma XL, Du J (2017) Cardiac fibroblast-specific activating transcription factor 3 protects against heart failure by suppressing MAP2K3-p38 signaling. *Circulation* 135: 2041–2057
- Lin X, Barravecchia M, Kottmann RM, Sime P, Dean DA (2019) Caveolin-1 gene therapy inhibits inflammasome activation to protect from bleomycin-induced pulmonary fibrosis. *Sci Rep* 9: 19643
- Lindquist JN, Marzluft WF, Stefanovic B (2000) Fibrogenesis - III. Posttranscriptional regulation of type I collagen. *Am J Physiol-Gastr L* 279: G471–G476
- Marone G, Galdiero MR, Pecoraro A, Pucino V, Criscuolo G, Triassi M, Varricchi G (2019) Prostaglandin D2 receptor antagonists in allergic disorders: safety, efficacy, and future perspectives. *Expert Opin Investig Drugs* 28: 73–84
- Marudamuthu AS, Bhandary YP, Fan L, Radhakrishnan V, MacKenzie B, Maier E, Shetty SK, Nagaraja MR, Gopu V, Tiwari N et al (2019) Caveolin-1-derived peptide limits development of pulmonary fibrosis. *Sci Transl Med* 11: eaat2848
- Maruyama T, Murata T, Ayabe S, Hori M, Ozaki H (2008) Prostaglandin D(2) induces contraction via thromboxane A(2) receptor in rat liver myofibroblasts. *Eur J Pharmacol* 591: 237–242
- Montgomery TA, Xu L, Mason S, Chinnadurai A, Lee CG, Elias JA, Cantley LG (2017) Breast regression protein-39/Chitinase 3-like 1 promotes renal fibrosis after kidney injury via activation of myofibroblasts. *J Am Soc Nephrol* 28: 3218–3226
- Nakagome K, Dohi M, Okunishi K, Tanaka R, Miyazaki J, Yamamoto K (2006) In vivo IL-10 gene delivery attenuates bleomycin induced pulmonary fibrosis by inhibiting the production and activation of TGF-beta in the lung. *Thorax* 61: 886–894
- Okamoto Y, Ninomiya H, Miwa S, Masaki T (2000) Cholesterol oxidation switches the internalization pathway of endothelin receptor type A from caveolae to clathrin-coated pits in Chinese hamster ovary cells. *J Biol Chem* 275: 6439–6446
- Ozono Y, Shide K, Kameda T, Kamiunten A, Tahira Y, Sekine M, Akizuki K, Nakamura K, Iwakiri H, Sueta M et al (2021) Neoplastic fibrocytes play an essential role in bone marrow fibrosis in Jak2V617F-induced primary myelofibrosis mice. *Leukemia* 35: 454–467
- Pedroza M, To S, Assassi S, Wu MH, Tweardy D, Agarwal SK (2018) Role of STAT3 in skin fibrosis and transforming growth factor beta signalling. *Rheumatology* 57: 1838–1850
- Phillips RJ, Burdick MD, Hong K, Lutz MA, Murray LA, Xue YY, Belperio JA, Keane MP, Strieter RM (2004) Circulating fibrocytes traffic to the lungs in response to CXCL12 and mediate fibrosis. *J Clin Invest* 114: 438–446
- Ray K (2015) Calcium-sensing receptor: trafficking, endocytosis, recycling, and importance of interacting proteins. *Prog Mol Biol Transl Sci* 132: 127–150
- Reilkoff RA, Bucala R, Herzog EL (2011) Fibrocytes: emerging effector cells in chronic inflammation. *Nat Rev Immunol* 11: 427–435
- Rockey DC, Bell PD, Hill JA (2015) Fibrosis—a common pathway to organ injury and failure. *N Engl J Med* 372: 1138–1149
- Safaeian L, Abed A, Vaseghi G (2014) The role of Bcl-2 family proteins in pulmonary fibrosis. *Eur J Pharmacol* 741: 281–289
- Saijou E, Enomoto Y, Matsuda M, Yuet-Yin Kok C, Akira S, Tanaka M, Miyajima A (2018) Neutrophils alleviate fibrosis in the CCl4-induced mouse chronic liver injury model. *Hepatol Commun* 2: 703–717
- Schlegel A, Arvan P, Lisanti MP (2001) Caveolin-1 binding to endoplasmic reticulum membranes and entry into the regulated secretory pathway are regulated by serine phosphorylation - protein sorting at the level of the endoplasmic reticulum. *J Biol Chem* 276: 4398–4408
- Shen YJ, Zuo SK, Wang YY, Shi HF, Yan S, Chen D, Xiao B, Zhang J, Gong YJ, Shi MH et al (2016) Thromboxane governs the differentiation of adipose-derived stromal cells toward endothelial cells in vitro and in vivo. *Circ Res* 118: 1194–1207
- Shenoy SK, Lefkowitz RJ (2011) beta-Arrestin-mediated receptor trafficking and signal transduction. *Trends Pharmacol Sci* 32: 521–533
- Singh D, Ravi A, Southworth T (2017) CRTH2 antagonists in asthma: current perspectives. *Clin Pharmacol* 9: 165–173
- Tager AM, LaCamera P, Shea BS, Campanella GS, Selman M, Zhao Z, Polosukhin V, Wain J, Karimi-Shah BA, Kim ND et al (2008) The lysophosphatidic acid receptor LPA(1) links pulmonary fibrosis to lung injury by mediating fibroblast recruitment and vascular leak. *Nat Med* 14: 45–54
- Tang J, Shen Y, Chen G, Wan Q, Wang K, Zhang J, Qin J, Liu G, Zuo S, Tao B et al (2017) Activation of E-prostanoid 3 receptor in macrophages facilitates cardiac healing after myocardial infarction. *Nat Commun* 8: 14656
- Tao X, Wang B, Zuo S, Yu Y (2021) Identification of prostaglandin receptor HA-tagged mice. *Sheng Li Xue Bao* (accepted Chinese version) <https://doi.org/10.13294/j.aps.2021.0050>
- Ueda S, Fukunaga K, Takihara T, Shiraishi Y, Oguma T, Shiomi T, Suzuki Y, Ishii M, Sayama K, Kagawa S et al (2019) Deficiency of CRTH2, a prostaglandin D2 receptor, aggravates bleomycin-induced pulmonary inflammation and fibrosis. *Am J Respir Cell Mol Biol* 60: 289–298

- Uller L, Mathiesen JM, Alenmyr L, Korsgren M, Ulven T, Hogberg T, Andersson G, Persson CG, Kostenis E (2007) Antagonism of the prostaglandin D2 receptor CRTH2 attenuates asthma pathology in mouse eosinophilic airway inflammation. *Respir Res* 8: 16
- Verma P, Tiwari M, Tiwari V (2018) In silico high-throughput virtual screening and molecular dynamics simulation study to identify inhibitor for AdeABC efflux pump of *Acinetobacter baumannii*. *J Biomol Struct Dyn* 36: 1182–1194
- Wang C, Wang H, Zhang D, Luo W, Liu R, Xu D, Diao L, Liao L, Liu Z (2018) Phosphorylation of ULK1 affects autophagosome fusion and links chaperone-mediated autophagy to macroautophagy. *Nat Commun* 9: 3492
- Wang M, Wey S, Zhang Y, Ye R, Lee AS (2009) Role of the unfolded protein response regulator GRP78/BiP in development, cancer, and neurological disorders. *Antioxid Redox Signal* 11: 2307–2316
- Wang XM, Zhang Y, Kim HP, Zhou Z, Feghali-Bostwick CA, Liu F, Ifedigbo E, Xu X, Oury TD, Kaminski N et al (2006a) Caveolin-1: a critical regulator of lung fibrosis in idiopathic pulmonary fibrosis. *J Exp Med* 203: 2895–2906
- Wang XM, Zhang YZ, Kim HP, Zhou ZH, Feghali-Bostwick CA, Liu F, Ifedigbo E, Xu XH, Oury TD, Kaminski N et al (2006b) Caveolin-1: a critical regulator of lung fibrosis in idiopathic pulmonary fibrosis. *J Exp Med* 203: 2895–2906
- Weder B, Mamie C, Rogler G, Clarke S, McRae B, Ruiz PA, Hausmann M (2018) BCL2 regulates differentiation of intestinal fibroblasts. *Inflamm Bowel Dis* 24: 1953–1966
- Weiskirchen R, Weiskirchen S, Tacke F (2019) Organ and tissue fibrosis: molecular signals, cellular mechanisms and translational implications. *Mol Aspects Med* 65: 2–15
- West C, Hanyaloglu AC (2015) Minireview: spatial programming of G protein-coupled receptor activity: decoding signaling in health and disease. *Mol Endocrinol* 29: 1095–1106
- Wynn TA, Ramalingam TR (2012) Mechanisms of fibrosis: therapeutic translation for fibrotic disease. *Nat Med* 18: 1028–1040
- Zhang Y, Stefanovic B (2016a) LARP6 meets collagen mRNA: specific regulation of type I collagen expression. *Int J Mol Sci* 17: 419
- Zhang YJ, Stefanovic B (2016b) LARP6 meets collagen mRNA: specific regulation of type I collagen expression. *Int J Mol Sci* 17: 419
- Zhu Y, Liao HL, Wang N, Yuan Y, Ma KS, Verna L, Stemerman MB (2000) Lipoprotein promotes caveolin-1 and Ras translocation to caveolae: role of cholesterol in endothelial signaling. *Arterioscler Thromb Vasc Biol* 20: 2465–2470
- Zuo S, Kong D, Wang C, Liu J, Wang Y, Wan Q, Yan S, Zhang J, Tang J, Zhang Q et al (2018a) CRTH2 promotes endoplasmic reticulum stress-induced cardiomyocyte apoptosis through m-calpain. *EMBO Mol Med* 10: e8237
- Zuo SK, Kong DP, Wang CY, Liu J, Wang YY, Wan QY, Yan S, Zhang J, Tang J, Zhang QQ et al (2018b) CRTH2 promotes endoplasmic reticulum stress-induced cardiomyocyte apoptosis through m-calpain. *EMBO Mol Med* 10: e8237